No number

Numerical Estimation of Asymmetry of In-Cylinder Flow in a Light Duty Direct Injection Engine with Reentrant Piston Bowl

Christian Ibron, Mehdi Jangi, Xue-Song Bai
Lund Institute of Technology, Sweden

Tommaso Lucchini
Politechnico Milano, Italy

ABSTRACT

Partially premixed combustion (PPC) can be applied to decrease emissions and increase fuel efficiency in direct injection, compression ignition (DICI) combustion engines. PPC is strongly influenced by the mixing of fuel and oxidizer, which for a given fuel is controlled mainly by (a) the fuel injection, (b) the in-cylinder flow, and (c) the geometry and dynamics of the engine. As the injection timings can vary over a wide range in PPC combustion, detailed knowledge of the in-cylinder flow over the whole intake and compression strokes can improve our understanding of PPC combustion. In computational fluid dynamics (CFD) the in-cylinder flow is sometimes simplified and modeled as a solid-body rotation profile at some time prior to injection in order to produce a realistic flow field at the moment of injection. In real engines the in-cylinder flow motion is governed by the intake manifold, the valve motion, and the engine geometry. The deviation of the real in-cylinder flow from a solid body rotation flow field varies with different piston positions. This paper reports on an CFD study of the formation and development of a real engine in-cylinder flow field in an optical light duty PPC engine from the opening of the intake valve at -360 CAD ATDC up to 20 CAD ATDC in a motored case (without fuel injection). The focus is put on the analysis of the temporal and spatial development of the swirl flow motion. The resulting flow field of the simulation is compared with the results from CFD simulation of an initially solid-body rotational flow in the cylinder. The adequateness of sector type mesh including solid-body rotation assumption as an initial flow is analyzed.

INTRODUCTION

Continuous increases in restrictions on NOx and soot emissions are driving the development of internal combustion engines. The fuel type and the mode of combustion are some of the most influential factors on emission levels of an engine and as such many new fuel types with corresponding combustion modes have been proposed over the years. Partially Premixed Combustion (PPC) is a combustion concept which employs early injection to generate a proper fuel/air mixing to allow for optimized heat release rate profile. This results in a reduced NOx emission due to low peak combustion temperature with low soot emissions owing to the premixed-dominated combustion environment. This concept was shown to be specially useful for the high octane number fuels, for example gasoline, cf., Kalghatgi et al. [3, 4]. The combustion process is rather sensitive to the injection strategy and the in-cylinder flow conditions. Manente et al. [6] showed that very high engine efficiency can be achieved by using high cetane number diesel-like fuels in PPC mode by suppressing the auto-ignition tendencies using Exhaust Gas Recirculation (EGR), which allows for the fuel to have sufficient time to mix with the air before the onset of ignition. The engine efficiency was shown to be as high as 57%.

The PPC combustion mode requires controllable incumbent time in order to mix a majority of the injected fuel into lean premixed or close to lean premixed state prior to the Start Of Combustion (SOC). During the incumbent time the level of fuel/air mixing is among other things dependent on the flow field in the cylinder. This has been investigated in light duty diesel engines among others by Perini et al. [7], whose experimental results and cylinder sector CFD simulations indicated that higher engine swirl numbers caused fuel rich pockets in the engine bowl to ignite first while low swirl numbers caused more fuel rich

pockets in the squish region where ignition occurred first Dempsey et al. [1] compared the full cylinder CFD simulations with sector mesh simulations for the equivalence ratio distribution and found that the results from the full cylinder simulations can be significantly different from the results from a sector mesh simulation. Zha et al. [13] and Perini et al. [8] performed CFD simulations of the formation and development of coherent structures (swirling flow) and the orientation of coherent structures in a light duty engine with re-entrant cylinder bowl. The results showed an asymmetric flow field which persisted through most of the compression stroke.

In order to understand the ignition and combustion process one must know the state of the fuel/air mixture (equivalence ratio) and the distributions of temperature and local turbulence prior to ignition. The work described in this paper aims to quantify the evolution of the in-cylinder flow in a light duty internal combustion engine. A portion of the intake manifold including the helical intake port of a 4 valve cylinder is studied in a 3D CFD simulation. The simulations are carried out for the intake stroke to establish the velocity, pressure and temperature fields inside the cylinder until Intake Valve Closing (IVC), and continued throughout the compression stroke. The geometry for the simulation is taken from intake and piston drawings for the engine used in the works of Tanov et al. [11, 12].

SETUP AND METHODOLOGY

ENGINE GEOMETRY The studied engine is a Volvo D5 2.5 liters light duty engine with a custom optical re-entrant piston bowl geometry. The experimental motored run was performed with a swirl flap covering the tangential port so only the helical port was included in the simulation. The full computational domain at bottom-dead-center (BDC) can be seen in Figure 1. The length of the intake manifolds above the valve is approximately 7 diameters of the intake manifolds, which allows for the flow to establish a reasonably developed profile close to the intake valve.

MESHING STRATEGY The simulations were performed using OpenFOAM^{TM} v2.2.x open source CFD software including Lib-ICE code library to handle moving engine topology provided and developed by Lucchini et al. [5]. The moving topology of the simulation domain was included by adapting the mesh node position to the topology changes. Node displacement was handled individually for each node and the magnitude and direction of the displacement was governed by a Laplace equation:

$$\nabla \cdot (\gamma \nabla \overline{u}) = 0 \tag{1}$$

where $\overline{u}$ is the velocity at which the mesh node is moving. The boundary condition of $\overline{u}$ was prescribed as follows: at the cylinder head the velocity was set to zero (the cell node would not move with time); at the piston surface the velocity was set to the same velocity of the piston; at the cylinder wall the velocity was set to be proportional to the piston velocity and the distance to the piston surface (to allow the nodes to slide on the wall). The diffusivity of each node γ was scaled with the nodes distance to the closest moving topology boundary. The node position ($\overline{x}_n$) in the time step $k+1$ was then calculated using:

$$\overline{x}_{n,k+1} = \overline{x}_{n,k} + \overline{u}\Delta t \tag{2}$$

Figure 1: Computational domain considered in this study. The intake, the valve, the cylinder, and the piston bowl geometries are shown.

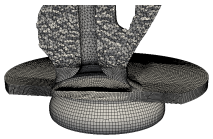

Figure 2: Mesh at initial time -360 CAD ATDC.

Since this method caused the mesh cells to deform over time a re-meshing strategy was required in order to maintain a high mesh quality. For every 20-30 crank angles of simulation, the flow field was interpolated onto a new mesh in which the simulation continued. In order to keep the mesh quality of the most deformed cells sufficiently high and the cell volumes sufficiently small, 7 mesh changes were used at the following intervals, -330, -300, -280, -250, -220, -200 and -190 CAD ATDC in the simulation of the intake stroke.

At all times in the simulation the largest cell size (below the cylinder head) was 1.0 mm and the gap between the valve and the valve seat was resolved by at least six nodes. For simplicity, at the intake valve opening (IVO) the gap was set to be 0.5 mm and the continued according to the valve motion profile. To resolve the valve gap at the initial conditions a hexahedral mesh was used as seen in Figure 2. At later stages the mesh was an auto-generated Cartesian mesh with tetrahedral adaptation at the boundaries, cf. Figure 3. This helped maintaining the mesh quality

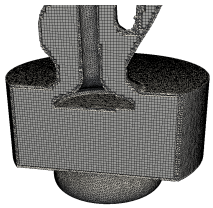

Figure 3: Mesh at time -300 CAD ATDC.

Stroke	92.3 mm
Bore	81 mm
Connecting rod	147 mm
Displacement	480 cm^3
Compression Ratio	1:11.3
Engine speed	800 rpm
Intake valve opening time	-360 CAD ATDC
Intake valve closing time	-164 CAD ATDC
Intake temperature	353 K
Intake pressure exp.	1.14 bar
Intake pressure sim.	1.10 bar
Experiment Swirl Number	2.6

Table 1: Characteristics of the engine taken from experiments of Tanov et al. [11].

despite the node movement.

PHYSICS MODELING The flow was simulated using unsteady Reynolds Averaged formulation of the Navier-Stokes equations (URANS) with the standard $\mathrm{k}-\epsilon$ turbulence model. Usage of URANS is justified by considering the simulation results as an ensemble average of an infinite number of engine cycles. This turbulence model employs a turbulent eddy diffusivity μ_T for modeling the Reynolds stresses. The turbulent eddy viscosity is modeled as $\mu_T = C_\mu \rho k^2/\epsilon$, where $C_\mu = 0.09$ is a model constant and ρ is the Reynolds averaged density of the gas mixture. The turbulent kinetic energy *k* and its dissipation rate ϵ are modeled using transported equations. The production of the turbulent kinetic energy is owing to the gradient of the mean flow velocity, while the dissipation of turbulent kinetic energy is due to viscous effect. Even though the $k-\epsilon$ model is not optimal for simulating rotating flows [9] due to the assumption about isotropic turbulence but its robustness and low computational cost makes it a common choice in combustion engine simulations.

INITIAL CONDITIONS Table 1 lists the engine geometrical details and operation conditions. The CFD simulation was initiated at the intake valve opening, i.e., in the present case, the piston at the TDC. The initial conditions of the simulation were set according to the experimental data of Tanov et al. [11]. Pressure in the cylinder domain downstream of the valve was set to 1 bar and at the inlet of the intake manifold the pressure was set to 1.1 bar. This is slightly lower than the reported intake pressure of 1.14 bar from the experiments [11]. The adjustment of the intake pressure was to match up with the in-cylinder pressure profile reported from the experiments. The cylinder mean flow was assumed to be a solid body rotation and the swirl number was set to 0.26 which is 10% of the experimental swirl number at BDC. In the intake manifolds upstream the valve the mean flow was set to zero and the intake flow is governed by the pressure gradient. The turbulent kinetic energy was initiated as 1 $\mathrm{m}^2/\mathrm{s}^2$ in the whole domain and 0.5 $\mathrm{m}^2/\mathrm{s}^2$ at the inlet. The dissipation rate of turbulent kinetic energy was initially set to a constant value of 450 $\mathrm{m}^2/\mathrm{s}^3$ in the domain and 700 $\mathrm{m}^2/\mathrm{s}^3$ at the inlet. Default OpenFOAM compressible flow wall functions were used at the wall boundaries.

ANALYSIS The swirling flow motion in the cylinder was often quantified using global parameters such as the engine swirl number. The swirl number is the ratio between the flows rate of rotation around the piston axis and the engine speed (RPM). One commonly used definition of the swirl number is [10]:

$$N_S = \frac{\dot{\omega}_{z,flow}}{\dot{\omega}_{piston}} = \frac{L_z/I_{zz}}{\mathrm{RPM}\cdot 2\pi/60} \tag{3}$$

where L_z is the the axial-component of the angular momentum vector L defined by:

$$L = \sum_{cells} \rho_{cell}\cdot V_{cell}\cdot \overline{r}_{o,cell}\times \overline{U}_{cell} \tag{4}$$

where subscript $cell$ denotes the condition evaluated at the center of the cell, V is the volume of the cell, $\overline{U}$ is the velocity vector in the cell, and $\overline{r}_{o,cell}$ is the distance vector from the center of mass to the cell,

$$\overline{r}_{o,cell} = \overline{r}_{cell} - \overline{r}_o \tag{5}$$

Here, $\overline{r}_{cell}$ and $\overline{r}_o$ are the position vectors of the cell center and the mass center of the considered domain, respectively. I_{zz} is the moment of inertia for the piston axis defined around the center of mass:

$$I_{zz} = \sum_{cells} \rho_{cell}\cdot V_{cell}\cdot (\overline{r}_{o,cell}\cdot \hat{e}_z)^2 \tag{6}$$

where $\hat{e}_z$ is the unit vector along the axis of the cylinder. The center of mass is calculated by:

$$\overline{r}_o = \frac{\sum_{cells}\rho_{cell}\cdot V_{cell}\cdot \overline{r}_{cell}}{\sum_{cells}\rho_{cell}\cdot V_{cell}} \tag{7}$$

Swirl number can not only be used to describe the swirling flow motion in the entire cylinder volume, which is typically done, it can also be used to describe the swirl motion in a cross sectional plane. By performing the summation in the above equations in a particular cross section a plane specific swirl number can be obtained, which is frequently used in the analysis of swirling burner flow where the swirl number is often defined at the burner exit plane.

The angular momentum vector describes the average direction of the rotation of the flow but it does not describe

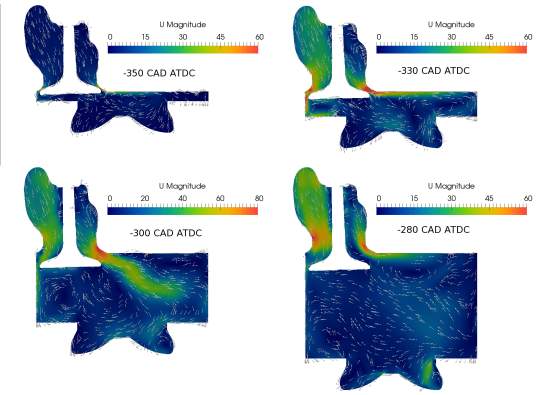

Figure 4: Velocity vectors colored with the magnitude of the velocity at -350 CAD ATDC (a), -330 CAD ATDC (b), -300 CAD ATDC (c) and -280 CAD ATDC (d). Velocity color scheme is scaled to show low speed flow structures; the maximum values of velocity is about 70 m/s.

the position of the swirling structure. Thus, in addition to the center of mass of a given domain, a center of rotation of the flow in the domain (the center of swirl) needs to be defined. In a solid-body rotational flow the center of the rotation is on the axis of the cylinder. However, in general cases the center of rotation is off the axis of the cylinder. Furthermore, there can be multiple rotational structures in the domain. Thus, the definition of the center of rotation is not trivial. In this study the center of rotation is defined using a function $f(\overline{r}_c)$, following the work of Michard et al. [2],

$$f(\overline{r}_c) = \frac{1}{N_{cells}} \sum_{cell}^{N_{cells}} \sin(\theta_{cell}) = \frac{1}{N_{cells}} \sum_{cell}^{N_{cells}} \frac{\left[(\overline{r}_{cell} - \overline{r}_c) \times \overline{U}_{cell}\right] \cdot \hat{e}_z}{\mid \overline{r}_{cell} - \overline{r}_c \mid\mid \overline{U}_{cell} \mid},$$

where θ_{cell} is the angle between the vectors $\overline{r}_{cell} - \overline{r}_c$ and $\overline{U}_{cell}$, and $\mid \overline{a} \mid$ is the length of vector $\overline{a}$. As seen, the dimensionless scalar function $f(\overline{r}_c)$ is bounded between -1 and 1. Its value depends on $\overline{r}_c$ selected. It can be shown that this bound is reached at the location of the vortex centre if the vortex is axisymmetrical [2]. For flows not axisymmetrical the center of rotation is at the maximum of absolute value of $f(\overline{r}_c)$. This method was applied in cross sectional planes cutting through the domain perpendicularly to the cylinder axis at intervals of 10 mm.

This type of definition can be applied to describe the tumble motion as well. Similar to the swirl number, a tumble number can be defined as the angular velocity vector around the radial direction. The projection of the angular momentum vector onto the radial plane indicates tumbling motion.

RESULTS AND DISCUSSION

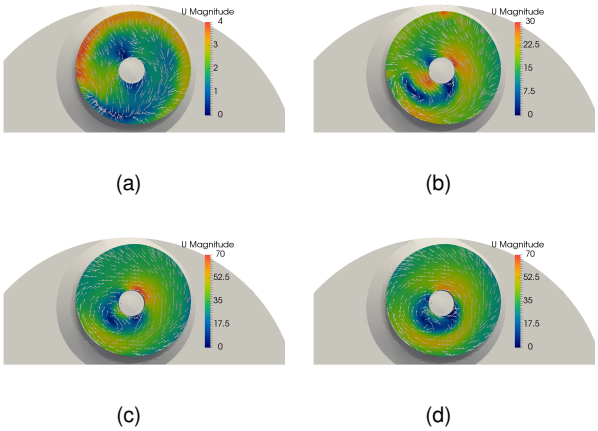

Figure 5: Velocity vectors in a cross section plane in the intake manifolds, 10 mm above the valve exit plane, at -350 CAD ATDC (a), -330 CAD ATDC (b), -300 CAD ATDC (c) and -280 CAD ATDC (d). The color indicates the magnitude of the velocity component in the horizontal plane.

EXPANSION CYCLE After the intake valve is opened the pressure difference between the inlet of the intake manifolds and the cylinder drives the air to flow into the cylinder. At -359.5 CAD ATDC (0.5 CAD after the valve opening) the flow speed around the valve can already reach Mach number of 1, owing to both the initial pressure difference and the narrow passway around the valve. As the valve is opened further the passway becomes wider and the pressure difference becomes smaller, the flow speed around the valve is decreased to below Mach number of unity. Figure 4 shows the velocity vector field at four different crank angles in the vertical plane crossing both the valve and the cylinder. The figure shows the development of the tumble flow structure inside the cylinder. At -350 CAD the piston is near the cylinder head, as such the flow is confined in the narrow squish volume. The flow on the left side of the valve forms a corner recirculation zone, while the flow on the right side of the valve continued in the direction parallel to the surface of the cylinder head and forms another recirculation zone. The flow velocity in the bowl is rather low, as indicated by the blue color in the figure. At -330 CAD the flow structure is further developed following that at -350 CAD. The piston is now at a larger distance from the valve and the cylinder head, thus, the recirculation zones are developed to a larger size, with the flow structures essentially similar to that at -350 CAD.

The tumble flow evolves into a different structure at -300 CAD. Due to the large cylinder volume the flow from the right side of the valve can now penetrate deeper into the cylinder volume. Associated with the highly penetrated flow stream large recirculation zones are established. At -280 CAD the tumble flow structure evolves further. The flow stream on the left side the valve is weaker and the corner recirculation zone is also weaker. The flow stream on the right side of the valve forms a recirculation zone in-between the valve and the valve seat, which pushes the flow stream to a narrow layer near the cylinder head.

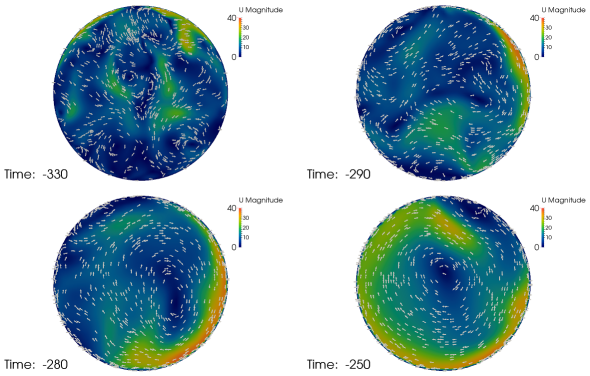

Figure 6: Velocity vectors in a cross section plane in the cylinder, in the middle between the cylinder head and piston surface, at -330, -290, -280, and -250 CAD ATDC.

The abrupt change of the tumble flow structure from -300 CAD to -280 CAD is attributed to the swirling flow developed in the intake manifolds and in the cylinder. Figure 5 shows velocity vector field in a horizontal cross section **10??? mm above the valve exit plane**. The figure illustrates the development of the swirling flow motion in the intake manifolds. At -350 CAD the flow is in the early development stage, and no significant swirl direction can be identified. At -330 CAD the flow is seen to develop into a swirling motion along clockwise direction; the flow in the lower left side of the figure forms a clockwise secondary vortex. From -330 CAD to -280 CAD the secondary vortex in the lower left side of the domain is progressively suppressed and eventually a stronger clockwise swirling flow motion is developed (cf. the difference in the velocity magnitude at different CAD). At -280 CAD the lower left side of the **valve rod** forms a low speed zone, which corresponds to the flow recirculation zone on the right side of the valve shown in Figure 4d. The development of the swirl flow motion in the intake is a result of the intake manifold geometry (cf. Fig. 1) and the position of the intake manifolds respect to the cylinder. The curvature of the intake manifolds causes the high velocity air of the intake flow to rotate very rapidly.

Figure 6 show the development of the swirling flow motion in the cylinder. At -330 CAD, multiple large-scale recirculation zones are seen; however, on significant swirling flow motion can be identified. From -290 CAD to -250 CAD the multiple recirculation zones merge gradually forming a clockwise swirling flow motion. Comparing with the development of the swirl flow motion in the intake manifolds the development of the swirl flow motion is later. The direction of the swirling flow in the cylinder is the same as that in the intake manifolds, which indicates the impact of the swirling flow motion in the intake manifolds on that in the cylinder.

Figure 7 shows the mean flow streamlines in the cylinder and the intake manifolds. It is seen that at -295 CAD the flow contains multiple three dimensional rotational structures, with certain swirling flow motion near the exit of the valve, but no dominant swirl direction in the main part

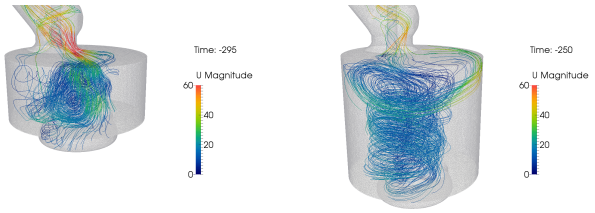

(a) (b)

Figure 7: Streamlines at (a) -295 CAD ATDC and (b) -250 CAD ATDC. A strongly tilted swirl kernel can be seen. The axis of the kernel is tilted more than 30 degrees to the piston axis.

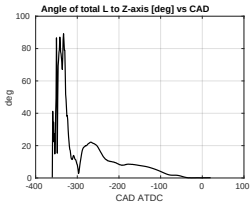

Figure 8: Angle of total angular momentum to cylinder axis. The orientation of the angular momentum vector shows the distribution between swirl and tumble motion. Full alignment to the cylinder axis means pure swirl.

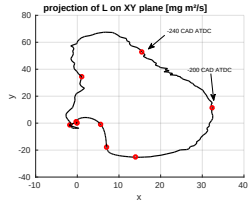

Figure 9: Projection of total angular momentum to plane perpendicular to cylinder axis. Intervals of 40 crank angles are marked with red rings.

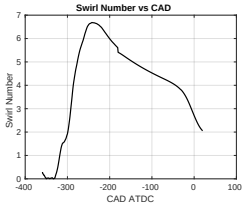

Figure 10: Development of swirl number. The total swirl number for this simulation is much higher than was expected from the experiments. This could possibly be due to the assumption that the swirl flap in the tangential port is fully blocking the flow which might not be the case.

of the cylinder. At -250 CAD a clear large-scale helical swirling flow structure can be identified. The mean axis of the rotational flow structure can be quantified using the angle between the angular momentum vector L and the axis of the cylinder. Figure 8 shows the evolution of the mean swirl directional angle. At -360 CAD (the initial condition) the in-cylinder flow was assumed to be a solid-body rotational flow with the axis of the rotation in align with the axis of the cylinder; thus, the initial angle is 0. After the intake valve is opened the swirl motion is evolved the swirl directional angle increases rapidly to above 80 degrees, as a result of the combination of the swirl motion and the tumble motion. One can see that the change of the angle is not monotonic with time, due to the rapid evolution of the tumble and swirl flow motion in the cylinder. After -320 CAD the swirl directional angle decreases rapidly and it maintains a value around 10 - 20 degrees throughout the remaining intake stroke.

Figure 9 shows the projection of the angular momentum L in the horizontal plane ($x - y$ plane). This figure shows both the direction of the rotational axis and the magnitude of the angular momentum. If the rotational axis is in align with the cylinder axis, the projection will be at $x = 0$ and $y = 0$, while a large deviation of the projection point from $x = 0$ and $y = 0$ requires both large swirl directional angle and large angular momentum. It is seen that at -360 CAD (the initial condition) the projection point is at $x = 0$ and $y = 0$, while is quickly deviate from its initial state. The variation of the projection point indicates that direction of the rotation axis of the incylinder flow varies with time.

The strength of the swirl motion can be characterized using the global swirl number defined in Eq. (3). Figure 10 shows the evolution of the global swirl number of the in-cylinder flow at different piston positions (excluding the intake flow). The initial swirl number was assumed to be 0.26, which is however quickly decreased to almost a value of zero, corresponding to the lack of swirl motion in the earlier intake stroke. After -320 CAD the flow is developing into swirl flow motion and the swirl number shows a rapid increase from zero to $6 - 7$. The maximal swirl number is found around -250 CAD, which is around the moment of the highest piston velocity; thereafter, the swirl number decreases with time, due to the slower velocity of the piston.

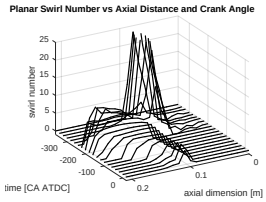

Figure 11: Planar swirl number at different axial position developing in time.

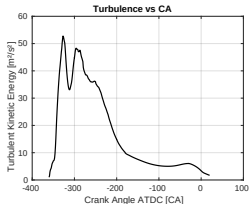

Figure 12: Development of volume averaged turbulent kinetic energy in the cylinder as a function of CAD.

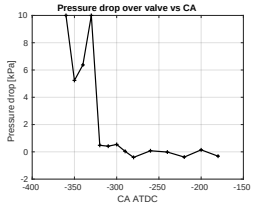

Figure 13: Pressure drop over valve as a function of CAD. The pressure drop was calculated as the average difference of two cross section surfaces perpendicular to the valve motion axis 1 cm above and 1 cm below the cylinder head.

Figure 11 shows the swirl number defined at the cross section plane in the intake manifolds and the cylinder. The axial distance $z = 0$ is defined at the cylinder head, while $z < 0$ is the intake manifolds and $z > 0$ represents the cylinder. The at the initial state (-360 CAD) the swirl number in the cylinder is 0.26, while in the intake manifolds the swirl number is zero (no flow motion). The swirl number in the intake manifolds increases rapidly to a value about 25 and maintained a much higher value throughout the intake stroke. As the intake flow approaches the the exit plane of the valve the swirl number shows a decrease due to the sudden expansion of the intake flow into the cylinder; further downstream in the cylinder the swirl number increases until very close to the piston.

The evolution of turbulent kinetic energy in the cylinder is displayed in Fig. 12. It is shown that the turbulent kinetic energy in the cylinder increases rapidly in the initial intake stage, from -360 CAD to about -320 CAD. Thereafter, the turbulent kinetic energy decreases, reaching a minimal value at around -310 CAD. Between -310 CAD and -280 CAD the turbulent kinetic energy increases again with increasing CAD, and thereafter the turbulent kinetic energy in the cylinder experiences a monotonic decrease during the intake stroke. The twin-peak behavior of turbulent kinetic energy is due to change of flow modes in the cylinder. During the first 40 crank angles (-360 CAD to -320 CAD) the pressure difference over the valve is much larger than

Figure 14: Streamlines at IVC. A strongly tilted swirl kernel can be seen.

that afterward, cf. Fig. 13. In this stage, The piston velocity is low and the in-cylinder flow is driven by the pressure difference between the intake and cylinder. The velocity gradient around the valve and in the recirculation zone in the cylinder allows the production of turbulence in this stage.

After -320 CAD the in-cylinder pressure becomes close to the intake pressure of 1.1 bar. The pressure difference between the intake and the cylinder is thus small, which results in a slower velocity around the valve and lower turbulence production rate. This is reason of the first peak of the turbulent kinetic energy shown in Fig. 12. In this stage the intake flow and the in-cylinder flow is driven by the piston motion. It is at this time (-330 to -250 CAD ATDC) that the flow begins to stabilize and a swirling motion is formed, cf. Fig. 6. From -320 CAD to -280 CAD the piston velocity increases with CAD, and as such the incylinder flow velocity and turbulent kinetic energy increase as well, as indicated by the second peak of turbulent kinetic energy around -280 CAD, cf. Fig. 12. After -270 CAD the piston velocity decreases with CAD, which gives rise to the decrease of the in-cylinder flow velocity and consequently the turbulent kinetic energy.

COMPRESSION CYCLE At IVC (-164 CAD ATDC) the intake flow is turned off. Figure 14 shows the the swirling flow motion. The axis of the rotation is noticeably tilted. As seen, in Figs. 8 and 9, as the piston compresses the in-cylinder flow the axis of the rotation is gradually becoming in alignment with the axis of the cylinder, which is due to the suppress of the tumble flow by the piston compression; thus, the flow becomes more similar to that of solid-body rotation. The swirl number decreases with CAD, owing to the loss of angular momentum due to the viscous dissipation effect, cf. Fig. 10. The motion of the piston starts to accelerate during the compression stroke, which increases the in-cylinder flow velocity and prevented the further decay of turbulent kinetic energy, cf. Fig. 12. It, however, does not promote the angular momentum and the decay of the swirl number.

At about -30 CAD ATDC the turbulent kinetic energy has a minor peak, which is due to the enhanced flow motion between the squish region and the bowl. Thereafter, the cylinder volume is small enough that the wall boundary layer viscous dissipation effect results in rapid decrease

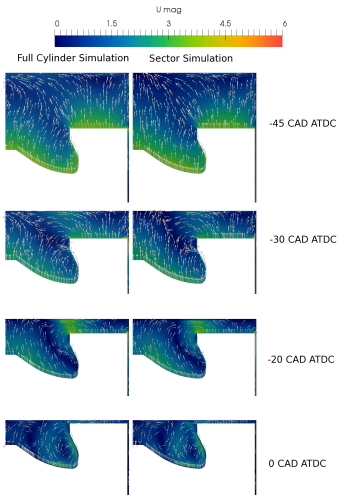

Figure 15: Comparison between the velocity vectors from CFD with the engine geometry and that from an initial solid-body rotational flow with a sector mesh.

in the both the turbulent kinetic energy and angular momentum (thus swirl number).

Dempsey et al [1] found significant effects of initial conditions on the equivalence ratio distribution with relatively late injections. It is expected that the asymmetric flow structure in the cylinder has rather important effect on the mixing of the fuel and air. This is specially true for early PPC injections such as SOI at -60 CAD ATDC or earlier. It is therefore interesting to investigate the evolution of a initial solid body rotational flow in the compression stroke and the difference between the solid-body rotational flow and that of the real flow considering the intake manifolds. To do this we have performed CFD simulation of an initially solid body rotational flow in the compression stroke. Due to axisymmetry the simulation was done in a sector mesh of ??? degrees. The initial turbulent kinetic energy and global swirl number are assumed to the same as that in the real engine simulation at IVC. Figure 12 shows that the evolution of turbulent kinetic energy in the cylinder is nearly identical to that of flow from the CFD simulation with the intake manifolds taking into account. The swirl number shown in Fig. 10 indicates that the decay rate of the swirl number in the solid body rotational flow is fairly similar to that of the real engine flow.

Figure 15 shows the comparison of the velocity vector field from the sector mesh and that from the full engine simulation. At -45 CAD and -30 CAD the full engine CFD results show a cross-axis flow motion while the sector mesh flow is parallel to the axis of the cylinder. The cross-axis flow stream was reported in the experiments of Tanov et al. [11], which is understood from the present work a result of the asymmetry of the axis of the large scale rotational flow structure. Other than the cross axis flow motion the major flow structure from the sector mesh is rather similar to that of the full engine flow simulation results.

CONCLUDING REMARKS CFD simulation of the in-cylinder flow was simulated with and without the consideration of the intake flow manifolds. The aims were to quantify the evolution of the tumble and swirl motion in the cylinder in the intake stroke and the compression stroke, and to discriminate the impact of the intake flow on the flow structures in the compression stroke. In PPC engines the mixing filed is believed to be sensitive to the flow and turbulence field, as such the often used assumption of the solid body rotational flow as the initial condition of compression stroke flow simulation may not be adequate. The main findings are summarized as follows:

- For the engine configuration studied in this work, the flow in the intake stroke is driven by two different mechanisms: (a) at the earlier intake stroke (from -360 CAD to -320 CAD ATDC) it is driven by the pressure difference between the intake and the cylinder, and (b) at later intake stroke (later than -320 CAD ATDC) the flow is driven by the piston motion. In the pressure drive stage the turbulent kinetic energy in the cylinder increases rapidly and then decays at the end of the pressure driven stroke. In the piston driven stage the turbulent kinetic energy in the cylinder increases with the piston velocity and then decreases as the piston is decelerated at the end of the intake stroke.
- The intake flow manifolds result in the formation of the swirl motion in the intake, which subsequently induces the formation of the swirl flow motion in the cylinder. In the pressure driven flow stage a strong tumble flow motion is generated in the cylinder and in the piston driven stage the swirl flow motion in the cylinder is developed. The swirl number increases with the piston velocity and decreases as the piston is decelerated in the later intake stroke.
- In the intake stroke the rotational flow structure is complex: the axis of the rotation is deviated from that of cylinder axis, and center of the rotation is not on the center of the axis. This asymmetric flow structure is maintained throughout the entire intake stroke and remains significant in the intake stroke as later as -30 CAD ATDC. It is envisaged that with earlier injection PPC (e.g. SOI at -60 CFD ATDC) the asymmetric flow motion could affect the mixing field.
- In the compression stroke, the tumble flow motion is suppressed and as such the flow approaches to the structure of solid body rotational flow, with the rotation axis in alignment with the cylinder axis. The cylinder volume averaged turbulent kinetic energy and the swirl number from CFD with the full engine geometry are in general on good agreement with that from the sector mesh CFD that assumes axi-symmetric solid body rotational initial flow. It is expected that for diesel injection near TDC, the assumption of slid-body rotational initial flow and sector mesh could be adequate.

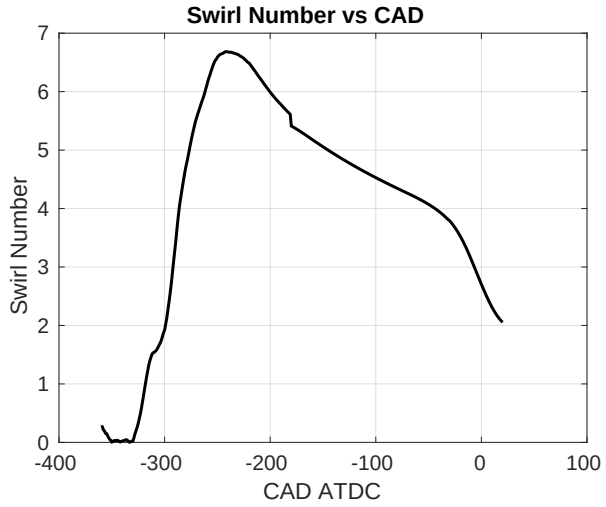

Figure 16: Development of swirl number. The total swirl number for this simulation is much higher than was expected from the experiments. This could possibly be due to the assumption that the swirl flap in the tangential port is fully blocking the flow which might not be the case.

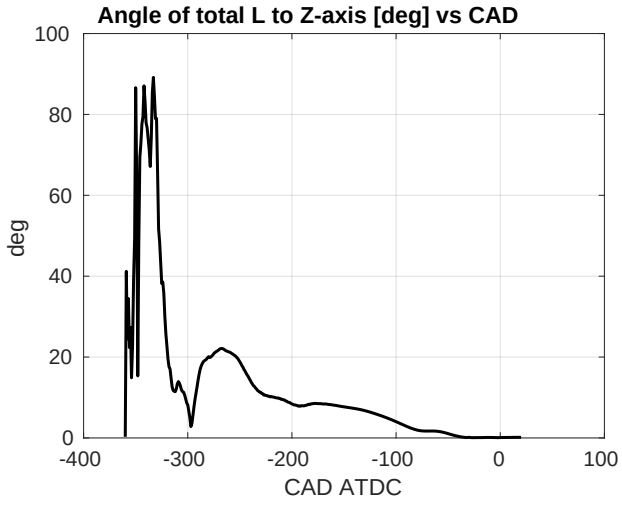

Figure 17: Angle of total angular momentum to cylinder axis. The orientation of the angular momentum vector shows the distribution between swirl and tumble motion. Full alignment to the cylinder axis means pure swirl.

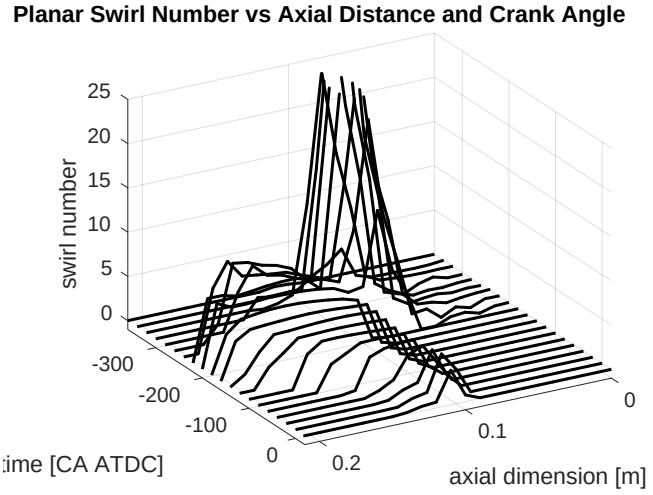

Figure 18: Planar swirl number at different axial position developing in time. The in-port planar swirl number shows the very high rotation which the flow experiences prior to passing through the valve. This explains the extreme horizontal direction of the flow seen in Figure XX.

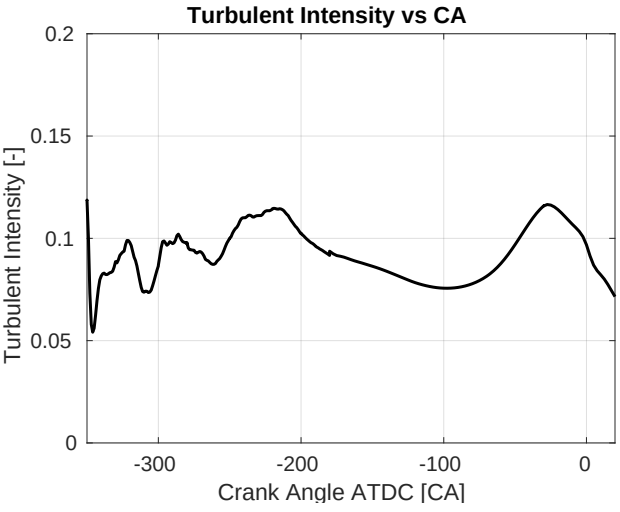

Figure 19: Favre averaged turbulent intensity inside the cylinder as a function of time. The instable behavior in the beginning is due to the interaction of piston motion to the valve motion (see pressure in Figure XX).

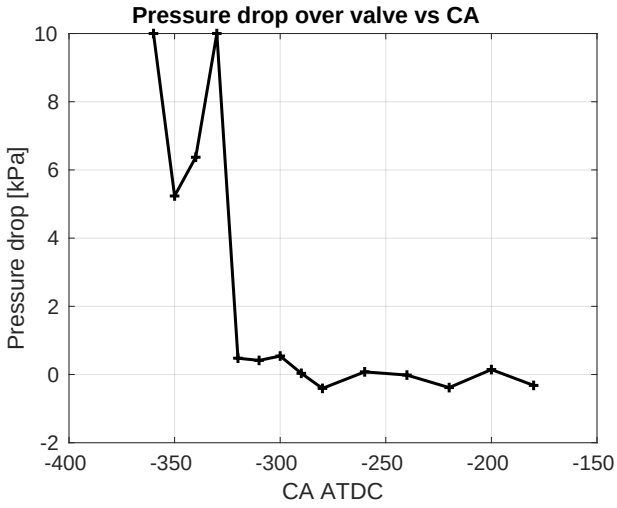

Figure 20: Pressure drop over valve as a function of CAD. The pressure drop was calculated as the average difference of two cross section surfaces perpendicular to the valve motion axis 1 cm above and 1 cm below the cylinder head. Instability in the initial crank angles is due to the interaction between accelerating piston and valve opening. The piston expands the volume flow faster than intake can fill up the cylinder initially.

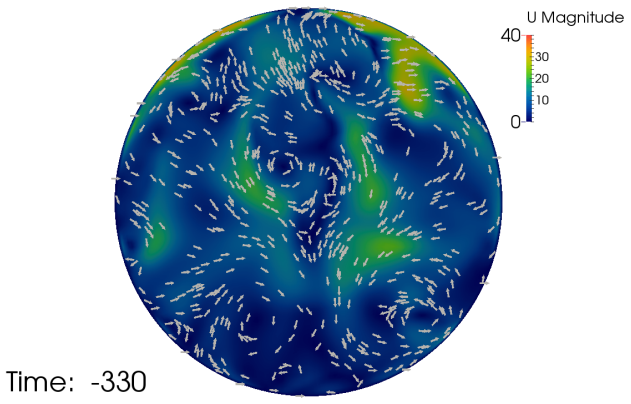

Figure 21: Planar velocity field in the middle of the cylinder at -330 CAD ATDC. Symmetric tendencies can be seen around the centerline.

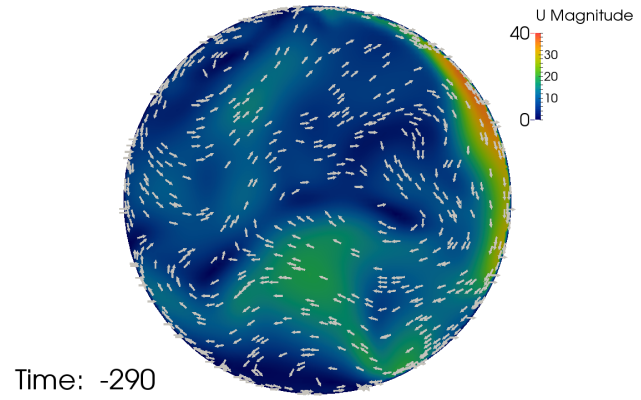

Figure 22: Planar velocity field in the middle of the cylinder at -290 CAD ATDC.

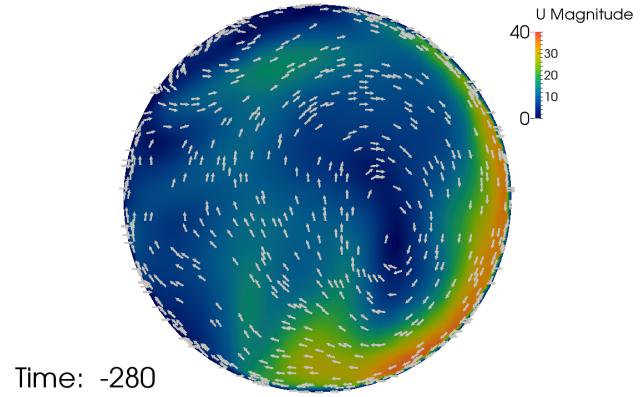

Figure 23: Planar velocity field in the middle of the cylinder at -280 CAD ATDC.

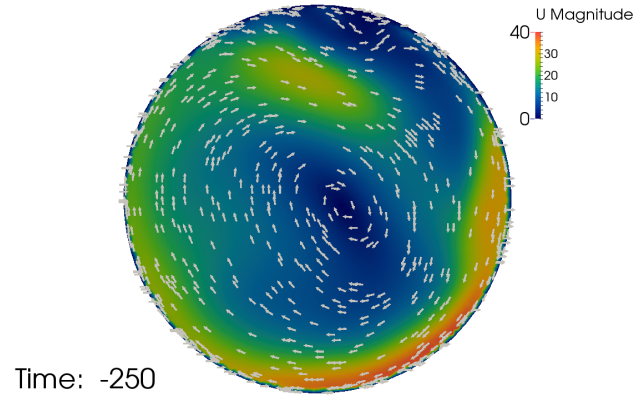

Figure 24: Planar velocity field in the middle of the cylinder at -250 CAD ATDC.

REFERENCES

[1] A. B. Dempsey, B.-L. Wang, R. D. Reitz, B. Petersen, D. Sahoo, and P. C. Miles, *Comparison of Quantitative In-Cylinder Equivalence Ratio Measurements with CFD Predictions for a Light Duty Low Temperature Combustion Diesel Engine*, SAE International Journal of Engines, 5 (2012), pp. 2012–01.

[2] L. Graftieaux, M. Michard, and N. Grosjean, *Combining PIV, POD and vortex identification algorithms for the study of unsteady turbulent swirling flows*, Measurement Science and Technology, 12 (2001), p. 1422.

[3] G. T. Kalghatgi, P. Risberg, and H.-E. Ångström, *Advantages of Fuels with High Resistance to Auto-ignition in Late-injection, Low-temperature, Compression Ignition Combustion*, SAE International, 3 2006.

[4] G. T. Kalghatgi, P. Risberg, and H.-E. ngstrm, *Partially Pre-Mixed Auto-Ignition of Gasoline to Attain Low Smoke and Low NOx at High Load in a Compression Ignition Engine and Comparison with a Diesel Fuel*, SAE International, 3 2007.

[5] T. Lucchini, G. D'Errico, and M. Fiocco, *Multi-Dimensional Modeling of Gas Exchange and Fuel-Air Mixing Processes in a Direct-Injection, Gas Fueled Engine*, SAE International, 3 2011.

[6] V. Manente, C.-G. Zander, B. Johansson, P. Tunestal, and W. Cannella, *An Advanced Internal Combustion Engine Concept for Low Emissions and High Efficiency from Idle to Max Load Using Gasoline Partially Premixed Combustion*, SAE International, 3 2010.

[7] F. Perini, A. Dempsey, R. Reitz, D. Sahoo, B. Petersen, and P. Miles, *A Computational Investigation of the Effects of Swirl Ratio and Injection Pressure on Mixture Preparation and Wall Heat Transfer in a Light-Duty Diesel Engine*, SAE Paper, 2013-01-11 (2013).

[8] F. Perini, P. C. Miles, and R. D. Reitz, *A comprehensive modeling study of in-cylinder fluid flows in a high-swirl, light-duty optical diesel engine*, Computers and Fluids, 105 (2014), pp. 113–124.

[9] S. B. Pope, *Turbulent Flows*, Cambridge University Press, 2000.

[10] F. Söderberg and B. Johansson, *Particle Image Velocimetry Flow Measurements and Heat-Release Analysis in a Cross-Flow Cylinder Head*, SAE International, 3 2002.

[11] S. Tanov, Z. Wang, H. Wang, M. Richter, and B. Johansson, *Effects of Injection Strategies on Fluid Flow and Turbulence in Partially Premixed Combustion (PPC) in a Light Duty Engine*, SAE International, 3 2015.

[12] Z. WANG, S. TANOV, H. WANG, M. RICHTER, B. JOHANSSON, AND M. ALDEN, *High-Speed Particle Image Velocimetry Measurement of Partially Premixed Combustion (PPC) in a Light Duty Engine for Different Injection Strategies*, SAE International, 3 2015.

[13] K. ZHA, S. BUSCH, P. C. MILES, S. WIJEYAKULASURIYA, S. MITRA, AND P. K. SENECAL, *Characterization of Flow Asymmetry During the Compression Stroke Using Swirl-Plane PIV in a Light-Duty Optical Diesel Engine with the Re-entrant Piston Bowl Geometry*, (2015), pp. –.